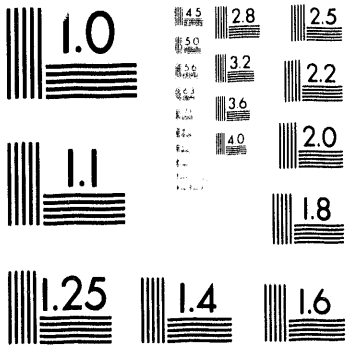
1.0
1.1
1.25
1.4
1.6
1.8
2.0
2.2
2.5
2.8
3.2
3.6
4.0
4.5
5.0

1 of 1

GA–A21415

THE ROLE OF THE RADIAL ELECTRIC FIELD IN CONFINEMENT AND TRANSPORT IN H–MODE AND VH–MODE DISCHARGES IN THE DIII–D TOKAMAK

by
P. GOHIL, K.H. BURRELL, E.J. DOYLE,*
R.J. GROEBNER, T.H. OSBORNE, and C.L. RETTIG*

This is a preprint of a paper to be presented at the Workshop on Local Transport Studies in Fusion Plasma, August 30 through September 3, 1993, in Varenna, Italy, and to be printed in the *Proceedings*.

Work supported by
U.S. Department of Energy
Contract Nos. DE-AC03-89ER51114 and DE-FG03-86ER53225

*University of California at Los Angeles.

GENERAL ATOMICS PROJECT 3466
AUGUST 1993

MASTER

GENERAL ATOMICS

78

THE ROLE OF THE RADIAL ELECTRIC FIELD IN CONFINEMENT AND TRANSPORT IN H-MODE AND VH-MODE DISCHARGES IN THE DIII-D TOKAMAK*

P. Gohil, K.H. Burrell, E.J. Doyle,† R.J. Groebner, T.O. Osborne, and C. Rettig†
General Atomics, P.O. Box 85608, San Diego, California USA 92186-9784

Measurements of the radial electric field, E_r, with high spatial and high time resolution in H–mode and VH–mode discharges in the DIII–D tokamak have revealed the significant influence of the shear in E_r on confinement and transport in these discharges. These measurements are made using the DIII–D Charge Exchange Recombination (CER) System.[1,2] At the L–H transition in DIII–D plasmas, a negative well-like E_r profile develops just within the magnetic separatrix. A region of shear in E_r results, which extends 1 to 2 cm into the plasma from the separatrix. At the transition, this region of sheared E_r exhibits the greatest increase in impurity ion poloidal rotation velocity and the greatest reduction in plasma fluctuations. A transport barrier is formed in this same region of E×B velocity shear as is signified by large increases in the observed gradients of the ion temperature, the carbon density, the electron temperature and electron density.[3-9] The development of the region of sheared E_r, the increase in impurity ion poloidal rotation, the reduction in plasma turbulence, and the transport barrier all occur simultaneously at the L–H transition. The localization of the sheared region in E_r is well defined with respect to the location of the separatrix, which is well resolved from the variation in the signal amplitudes of the CER chords spanning the separatrix.[7] Progressing into the H–mode, the transport barrier and the improved confinement lead to large impurity ion edge pressure gradients, which reinforce the shear in E_r just within the separatrix and provide conditions favorable for maintaining the H–mode.[7] A further improvement in confinement, known as the VH–mode, is observed when the shear in E_r penetrates further into the plasma interior.[10] This penetration is determined from the increase in the shear in the impurity ion toroidal rotation velocity profile in the transition from the H–mode to the VH–mode. The increase in the spatial extent of the E×B velocity shear correlates with a reduction of high frequency density fluctuations and the effective single fluid thermal diffusivity, χ_{eff}, over this same region.[11] This region of increased penetration of E_r shear defines the plasma volume which exhibits the substantial increase in confinement observed in VH–mode plasmas.[10-12]

The L–H transition occurs in a very narrow region ($\lesssim$2 cm) just within the plasma separatrix and investigations of the local transport at the transition require measurements of kinetic profiles [$T_i(r)$, $n_{C\,VI}(r)$, $T_e(r)$, $n_e(r)$] with sufficient spatial resolution (<1 cm) to adequately determine the changes involved. The DIII–D CER system has an effective

* This work was supported by the U.S. Department of Energy Contract Nos. DE-AC03-89ER51114 and DE-FG03-86ER53225.

† Present address: Electrical Engineering Department and IPFR, University of California, Los Angeles, California USA 90024-1594.

spatial resolution of 6 mm for E_r and plasma velocity measurements and a resolution of 3 mm for ion temperature and carbon density measurements. These measurements have determined the formation and the nature of the transport barrier at the transition. The development of the spatial structure of the radial electric field, E_r, at the L–H transition is clearly shown in Fig. 1(a). The measurements of E_r are determined from spectroscopic measurements of the C VII impurity ion obtained from the DIII–D CER system and the radial force balance equation.[7] E_r is essentially zero throughout the L–mode phase as is indicated by the profile at 7 ms before the transition. At the L–H transition, the radial electric field just inside the separatrix becomes significantly negative and there is a clear development of a negative well-like structure in the E_r profile within the 2 cm of the separatrix. This region of sheared E_r then persists into the H–mode as shown by the later time profile. The greatest contribution to E_r in the radial force balance equation comes from the poloidal rotation of the C VII ions which increases dramatically at the transition as shown in Fig. 1(b). Also, shown on both figures is the change in density fluctuations at the plasma edge as determined from the reflectometry system.[13] This change is represented by the radial profile of the ratio of the frequency integrated reflectometer power levels after the transition compared to before the transition. This ratio is determined for each reflectometer channel observing the plasma edge. The locations of the reflectometer points are determined using the electron density profiles measured by the DIII–D Thomson scattering system.[14] Figure 1(a) clearly shows that the region of the sheared electric field is also the region of the greatest reduction in density fluctuations. Figure 1(c) and 1(d) show the ion temperature and C VII density profiles for those same times. There is an increase in the gradients of the ion temperature and carbon density at the transition with further increases in time into the H–mode. Similarly, Figs. 1(e) and 1(f) show the steepening gradients of the electron temperature and density profiles as determined by the Thomson scattering system. The steepening of the gradients is a clear indication of the formation of transport barrier for the ions and the electrons at the plasma edge. The regions of the sheared electric field, the reduction in the plasma density fluctuations, and the transport barrier are the same and form simultaneously at the L–H transition.

It should be noted that the most rapid change in the kinetic profiles at the transition are observed at the very edge of the plasma. The reduction of the average thermal diffusivities and the improved confinement further in towards the plasma core occurs on a much slower timescale of at least a factor 100 on the order of 10s of milliseconds.[15]

The region of the shear in E_r and the transport barrier both form just inside the last closed flux surface (LCFS). The localization of this region with respect to the LCFS is well-defined from analysis of the amplitudes of the CER spectra observed by the edge spatial chords. Figure 2 shows the amplitude of the CER signal from four spatial channels as a function of time for a hot ion H–mode plasma. Each spatial channel is separated by 6 mm in radial position. The location of the separatrix as determined from magnetic measurements and an MHD equilibrium code[16] (EFIT) is 2.287 ± 0.005 m. Chords V11 and V12 are inside the separatrix and Chords V13 and V14 are on or outside the separatrix. At the L–H transition, Chords V11 and V12, which are inside the separatrix show increases in signal amplitude after the L–H transition whereas Chords V13 and V14 show a clear decrease in signal amplitude. Furthermore, the

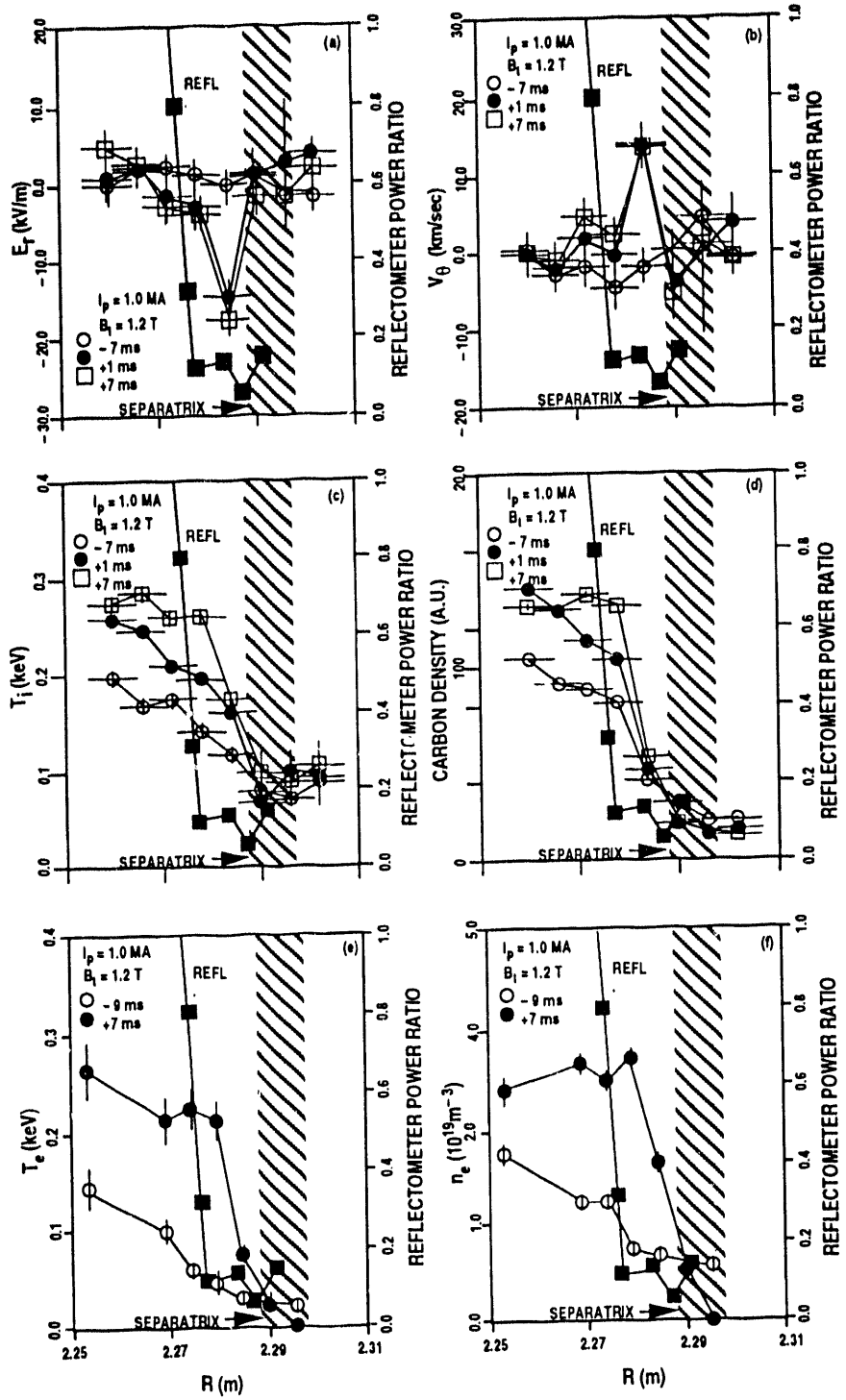

Fig. 1. Radial profiles of various quantities at the plasma edge for three times spanning the L–H transition. The horizontal axis represents the major radius of the measurement. The shaded region represents the uncertainty in the determination of the separatrix location from magnetic measurements and MHD equilibrium fits. Also shown in each subfigure is the change in the power of the density fluctuation signal measured by the reflectometry system across the transition. This change is shown as the ratio of the reflectometer power after the transition to before the transition. The vertical scale for this measurement is shown on the right hand side of the figure. The times shown in the figures are with respect to the time of the L–H transition. The integration time of the CER measurements is 2 ms. The subfigures are: (a) profile of the radial electric field, (b) profile of the poloidal rotation velocity of the C VII ions, (c) profile of the ion temperature, (d) profile of the density of C VII ions, (e) electron temperature profile as measured by the Thomson scattering system, (f) electron density profile as also measured by the Thomson scattering system.

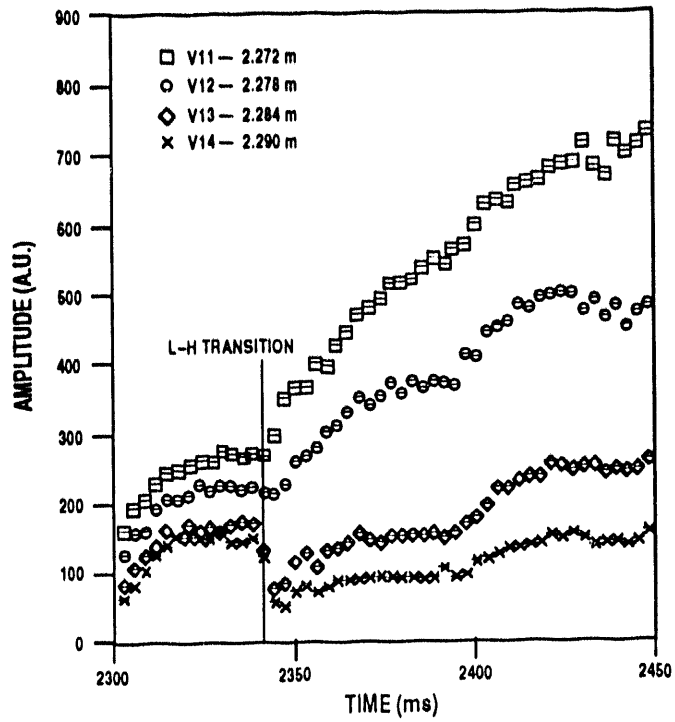

Fig. 2. The amplitudes of the actual CER signal for four poloidal Chords V11 to V14 as a function of time from the L-mode and through the H-mode. The deuterium beams for auxiliary heating were turned at 2300 ms and the L-H transition occurred at 2340.5 ms, followed by an uninterrupted H-mode phase to 2450 ms. The chord's amplitudes have undergone a relative calibration and a normalization. The V11 chord is the innermost chord and V14 is the outermost chord. The chord separation is 0.6 cm.

difference between the amplitude of Chords V12 and V13 increased dramatically at the transition and into the H-mode indicating the formation of a strong particle transport barrier and high C VII density gradients just within the separatrix. The variation in the signal amplitudes of the CER channels show agreement with the EFIT results on the location of the separatrix within the error bar of the EFIT determination. The change in signal amplitudes for chords inside and outside the separatrix location is significant and is a clear signature of the L–H transition.

The ion temperature and carbon density gradients just inside the separatrix continue to evolve over 10s of milliseconds into the H-mode, which result in large carbon ion pressure gradients at the plasma edge. Also, the carbon ion toroidal rotation across the plasma increases with time into the H-mode such that later in the H-mode the toroidal rotation contribution to E_r from the force balance equation cancels out the poloidal rotation term just inside the separatrix. However, the well-developed shear in E_r is maintained as a result of the large negative pressure gradient at the plasma edge throughout the H-mode.[7]

The progression from H-mode to VH-mode plasmas is marked by an increase in energy confinement time which can be up to 2.4 times the JET/DIII-D ELM-free H-mode scaling relationship. The H-mode to VH-mode transition occurs when the region of high shear in the radial electric field at the plasma edge extends further into the plasma core.[10] Transport analysis using the ONETWO transport code[17] indicates that the region which exhibits the largest increase in E_r shear towards the plasma core (between magnetic flux surfaces, ρ = 0.6 to 0.9) corresponds to the region of decreased local

thermal transport in the VH–mode. Figure 3 shows the development of the E_r profile from H–mode (t = 2140 ms) to VH–mode (t = 2490 ms) conditions. The region of high E_r shear typical of H–mode extends from $\rho = 0.9$ to the separatrix. In VH–mode, this region of high shear has extended inwards to $\rho = 0.6$. The determination of the effective single fluid thermal diffusivity, χ_{eff}, for these two times clearly shows a significant improvement in thermal transport over this same region.[11] As a measure of the effectiveness of the increased E_r shear in reducing the plasma turbulence, the expression of Biglari, Diamond and Terry[18] for the magnitude of shear required for turbulence suppression is used, $V'_{E\times B} \equiv (B/B_T)\, d/dR\, (E_r/B) \geq (\Delta\omega/k_\theta \Delta R) \equiv V'_{BDT}$ where B is the total magnetic field, B_T is the toroidal component, $\Delta\omega$ is the frequency spread of the turbulence, ΔR is the radial correlation length and k_θ is the poloidal wavenumber of the turbulence. Measurements of these quantities in the plasma edge of DIII–D[8] give $\Delta\omega \approx 2\pi \times 100$ kHz and $\Delta R \approx 1$ cm for $k_\theta = 2$ cm^{-1}, which then gives $V'_{BDT} \approx 3 \times 10^5$ s^{-1}. Using these edge conditions as an approximation to conditions further in, the central part of Fig. 3 shows that the measured increase in E_r shear is sufficient to suppress the turbulence between $\rho = 0.6$ to 0.9, which is also the region of improved thermal transport.

Burst-like density fluctuations, measured by the FIR scattering system[9] in the range of 0.5 to 1.5 MHz Doppler shifted (in lab frame) and also by the soft X–ray system and the magnetic probes, are observed to decrease around $\rho \approx 0.8$ as the E_r shear broadens. At the same time, there is a marked increase in the shear of the toroidal velocity between $0.67 < \rho < 0.82$, whereas the toroidal velocity between $0.93 < \rho < 0.82$ slows down about 20 ms before the improvement in thermal transport. Because these bursts transport angular momentum, these fluctuations are referred to as momentum transfer events

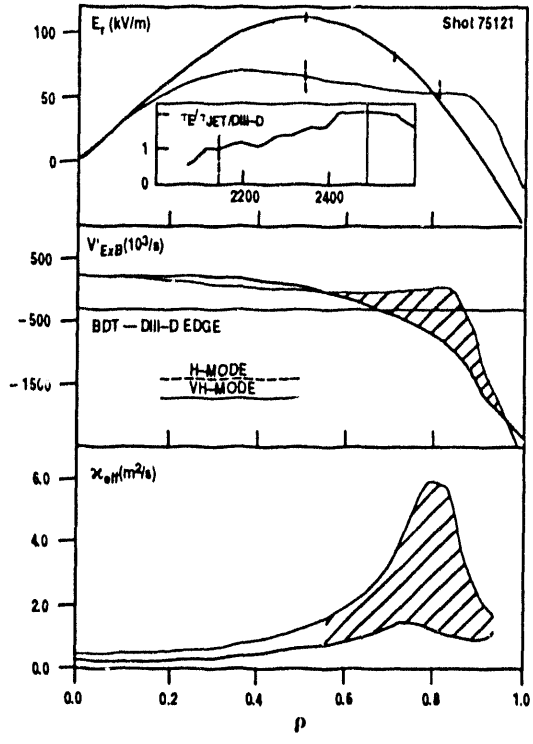

Fig. 3. Radial profiles of the radial electric field, the shear in the E×B velocity and the single fluid thermal diffusivity at an H–mode time and VH–mode time of Shot 75121. The solid (VH–mode) and dash (H–mode) curves represent the times shown in the inset in the top box which shows the history of the thermal energy confinement time normalized to the JET/DIII–D H–mode scaling relationship.

(MTEs).The large increase in energy confinement follows after the expansion of the region of high shear in E_r and the reduction of the density fluctuations. It should be noted that although suppression of MTEs results in improved confinement, the increase in velocity and E_r shear and energy confinement times can occur prior to significant suppression of MTEs in cases where the MTEs are weak.

VH–mode plasmas in DIII–D are most prevalent in high triangularity, double-null diverted configurations. In these configurations, a large part of the plasma volume accesses the second stable regime to ideal ballooning modes.[12] Consequently, VH–mode plasmas are ELM-free and do not suffer from confinement losses due to ELMs. Although access to the second stable regime to ideal ballooning modes may be a necessary condition for VH–mode, it is not a sufficient condition. The accessibility of the plasma to the stable regime is insufficient for the observed confinement improvement since the second stable regime is only accessed in the region between $\rho \approx 0.85$ and the separatrix, whereas the large decrease in the thermal diffusivity is observed primarily between $0.6 < \rho < 0.9$. Therefore, it does not appear that access to the second stable regime alone is the reason for the observed improvement in confinement.

Measurements of the radial electric field, plasma turbulence, thermal transport, and energy confinement have been performed for a wide range of plasma conditions and configurations. The results support the supposition that the progression of improving confinement at the L–H transition, into the H–mode and then into the VH–mode can be explained by the hypothesis of the suppression of plasma turbulence by the increasing penetration of the region of sheared E×B velocity into the plasma interior.

REFERENCES

1 Gohil, P., K.H. Burrell, R.J. Groebner, et al., Rev. Sci. Instrum. **61** (1990) 2949.

2 Gohil, P., K.H. Burrell, R.J. Groebner, et al., in Fusion Engineering (Proc. 14th IEEE/NPSS Symp. California, 1991) Vol. 2, IEEE, New Jersey (1992) 1199.

3 Burrell, K.H., T.N. Carlstrom, E.J. Doyle, et al., Phys. Fluids B **2** (1990) 1405.

4 Groebner, R.J., W.A. Peebles, K.H. Burrell, et al., Plasma Physics and Controlled Nuclear Fusion Research 1990, Vol. 1, IAEA, Vienna (1991) 453.

5 Burrell, K.H., T.N. Carlstrom, E.J. Doyle, et al., Plasma Physics and Controlled Fusion. **34** (1992) 1859.

6 Gohil, P., K.H. Burrell, E.J. Doyle, et al., in Controlled Fusion and Plasma Physics (Proc. 18th European Conf. Berlin, 1991) Vol. 15C, Part I, EPS, (1991) 289.

7 Gohil, P., K.H. Burrell, E.J. Doyle, et al., General Atomics Report GA-A21265 (1993); submitted to J. Nucl. Fusion.

8 Doyle, E.J., C.L. Rettig, K.H. Burrell, et al., in Plasma Physics and Controlled Nuclear Fusion Research (Proc. 14th Int. Conf. Wurzburg 1992) Vol. 1, IAEA, Vienna (1993) 235.

9 Rettig, C.L., W.A. Peebles, K.H. Burrell, et al., J. Nucl. Fusion **33** (1993) 643.

10 Burrell, K.H., T.H. Osborne, R.J. Groebner, et al., to be published in the Proc. 20th European Conf. on Controlled Fusion and Plasma Heating, Lisboa, Portugal (July 26–30, 1993).

11 Osborne, T.H., K.H. Burrell, T.N. Carlstrom, et al., General Atomics Report GA-A21182 (1992); submitted to Nucl. Fusion.

12 Greenfield, C.M., B. Ballet, K.H. Burrell, et al., to be published in the Proc. 20th European Conf. on Controlled Fusion and Plasma Heating, Lisboa, Portugal (July 26–30, 1993).

13 Doyle, E.J., T. Lehecka, N.C. Luhmann, et al., Rev. Sci. Instrum. **61** (1990) 3016.

14 Carlstrom, T.N., G.L. Campbell, J.C. Deboo, et al., Rev. Sci. Instrum. **61** (1990) 3016.

15 Kurki-Suonio, T.K., K.H. Burrell, R.J. Groebner, et al., J. Nucl. Fusion **33** (1993) 301.

16 Lao, L.L., J.R. Ferron, R.J. Groebner, et al., Nucl. Fusion **30** (1990) 1035.

17 Pfeiffer, W., F.B. Marcus, J.C. Armentrout, et al., J. Nucl. Fusion **25** (1985) 655.

18 Biglari, H., P.H. Diamond, P.W. Terry, et al., Phys. Fluids B **2** (1990) 1.

DATE
FILMED
12/27/93
END